Vietnam Journal of Science and Technology
DOI: https://doi.org/10.15625/2525-2518/21896

Batch to continuous photocatalyst degradation of oxytetracycline using g-C_3N_4/Bi_2MoO_6/Clinoptilolite nanocomposite and application in lake water

Phuong Thu Le[1], Ngoc Thanh Truc Nguyen[1], Hong Nam Nguyen[1], Trung Dung Nguyen[2], Thu Phuong Nguyen[1], Tien Le[1], Thi Mai Thanh Dinh[1,*]

[1]*University of Science and Technology of Hanoi, Vietnam Academy of Science and Technology, 18 Hoang Quoc Viet Street, Nghia Do Ward, Ha Noi, Viet Nam*
[2]*Le Quy Don Technical University, 236 Hoang Quoc Viet Street, Nghia Do Ward, Ha Noi, Viet Nam*

[*]Email: *dinh-thi-mai.thanh@usth.edu.vn*

Received: 4 November 2024; Accepted for publication: 10 January 2025

Abstract. Oxytetracycline (OTC) is widely used in aquaculture; however, increasing residue in water has contributed to antibiotic pollution and increased antibiotic resistance. A novel nanocomposite material - g-C_3N_4/Bi_2MoO_6/Clinoptilolite (CNBC), has been demonstrated to effectively degrade OTC in water via photocatalysis in both batch and continuous systems. The composite material was successfully synthesized by the solvo-thermal process under the conditions of (a precursor ratio of 14:56:30 (g-C_3N_4:Bi_2MoO_6:Clinoptilolite). Physicochemical characterization results (FT-IR, XRD and FE-SEM, and EDX) showed that g-C_3N_4/Bi_2MoO_6 was homogeneously dispersed on the surface of Clinoptilolite. The OTC degradation efficiency was 100 % with a catalyst content of 150 mg/L, while with 500 mg/L the efficiency was only 85.81 % in the batch system. These results suggest that this nanocomposite could be an effective solution for removing OTC from water on an industrial scale, helping to solve the problem of antibiotic pollution in the aquatic environment.

Keywords: oxytetracycline, continuous photocatalytic system, g-C_3N_4/Bi_2MoO_6/Clinoptilolite nanocomposite.

Classification numbers: 2.4.2, 3.4.2, 3.7.3.

1. INTRODUCTION

Oxytetracycline (OTC) is a first-generation tetracycline antibiotic recognized for its broad-spectrum activity against a wide array of micro-organisms, including both Gram-negative and Gram-positive anaerobic bacteria. Its low cost has promoted its extensive use in both human and veterinary medicine, particularly in aquaculture [1]. OTC was the first antibacterial agent approved by the USFDA for finfish aquaculture. Currently, in the United States, OTC is now allowed to treat infections caused by Aeromonas, Pseudomonas, and Haemophilus bacteria in salmonids and channel catfish [2]. In Viet Nam, over 72 % of shrimp farmer in the upper Mekong Delta have been using OTC antibiotics to prevent diseases in aquaculture [3,4]. However, OTC is not fully metabolized in treated animals, with over 75 % being excreted in its

UNCORRECTED PROOF

active form, potentially contaminating the environment and posing health risks such as central nervous system disorders, endocrine disruption, and nephropathy [5]. The lack of stringent regulations governing antibiotic use in Viet Nam's aquaculture industry has exacerbated the environmental accumulation of antibiotics residues. The total concentration of antibiotic residues, including OTC, was found to be 2,240 ng/L in 13 lakes in Hanoi in 2024. Reported OTC concentrations in Viet Nam included 76,800 ng/L in wastewater [6], 4.24 ng/L in aquaculture effluents, 30 µg/L in livestock wastewater, and 17.78 ng/L in household wastewater [7]. In food sample, OTC levels in pork and chicken samples ranged from 1.1 to 12.9 µg/g [8]. In contrast, in China, the maximum permissible OTC concentration in wastewater was from 0.1 µg/L to 5.5 µg/L. Several lakes in China contain OTC, including Honghu Lake, China (217.9 ng/L on average, ranging from 36 to 2,199.5 ng/L) [9], Bosteng Lake, China (up to 6.6 ng/L) [10], Chaohu Lake, China (up to 2.5 ng/L) [11], and Taihu Lake (44.2 ng/L on average, with a maximum of 72.8 ng/L) [12]. The widespread and indiscriminate application of OTC in both human and veterinary medicine has significantly contributed to the accumulation of OTC residues in the environment, creating selective pressure that facilitates the survival and proliferation of resistant strains. Consequently, it is crucial to effectively remove OTC residues from aquatic environments. Various methods for OTC degradation have been explored, including adsorption [13], biological processes [14], and advanced oxidation techniques [15]. Among these, photocatalytic degradation has proven to be particularly effective for breaking down pollutants that are present at high concentrations, exhibit structural complexity, or have low biodegradability [16].

The research paper reported that Bi_2MoO_6 and g-C_3N_4 form an effective Z-scheme heterojunction [10,17], and when combined with $Na_2S_2O_8$ [18], it enhances photocatalytic degradation. Therefore, a system using g-C_3N_4, Bi_2MoO_6, $Na_2S_2O_8$, and visible light can minimize charge carrier recombination and promote both oxidation and reduction reactions to produce $SO_4^{\bullet-}$, $^{\bullet}OH$, and $O_2^{\bullet-}$ radical for efficient pollutant degradation [19]. However, g-C_3N_4 tends to stack in layered wrinkled formation, while Bi_2MoO_6 forms 3D flower-like spherical crystals, which can aggregate easily. Clinoptilolite, with its large surface area, primarily facilitates photocatalytic reactions on the material's surface. Therefore, combining g-C_3N_4, Bi_2MoO_6, and Clinoptilolite increases the overall surface area, enhancing adsorption capacity and improving degradation efficiency in the CNBC system [19].

This article introduces a novel approach to the photocatalytic degradation of oxytetracycline (OTC) using a g-C_3N_4/Bi_2MoO_6/Clinoptilolite nanocomposite, showcasing an innovative transition from batch to continuous processing systems. The creativity of this study lies in optimizing the photocatalyst synthesis process at large scale, combining the unique properties of each component to enhance degradation efficiency and operability. Furthermore, the development of a scalable continuous system represents a significant advancement in the application of photocatalytic technologies for real-world water treatment scenarios, providing a sustainable solution to antibiotic pollution. This creative integration of materials science and engineering paves the way for future innovations in environmental remediation technologies. In this study, the effectiveness of a a g-C_3N_4/ Bi_2MoO_6/ Clinoptilolite nanocomposite in degrading oxytetracycline (OTC) in water systems through photocatalysis, exploring the potential of transitioning from batch to continuous systems.

UNCORRECTED PROOF

2. MATERIALS AND METHODS

2.1. Chemical reagents

All the chemicals utilized in the research were of analytical grade and obtained without further purification. Natural clinoptilolite was obtained from Turkey. Bismuth nitrate pentahydrate ($Bi(NO_3)_3.5H_2O$), sodium molybdate dihydrate ($Na_2MoO_4.2H_2O$), ethylene glycol ($C_2H_4(OH)_2$), ethanol (C_2H_5OH), and urea (CH_4N_2O) were purchased from Merck (USA). Additionally, sodium hydroxide (NaOH) and sulfuric acid (H_2SO_4) from Merck are used for pH adjustment. Furthermore, oxytetracycline (OTC) was supplied from Sigma (USA). Double distilled water was used throughout all the experiments.

2.2. Synthesis of the g-C_3N_4/ Bi_2MoO_6/ Clinoptilolite nanocomposite

g-C_3N_4/ Bi_2MoO_6/ Clinoptilolite (CNBC) nanocomposites were produced using modified solvothermal methods. This study significantly improves the earlier synthesis process [19]. The precursor ratio for the g-C_3N_4/ Bi_2MoO_6/ Clinoptilolite nanocomposite was 14:56:30. This study raised precursor levels by 8-fold and solvent volume by 4-fold (ethanol and ethylene glycol, 1:1 ratio) compared to Le's method [19]. The chemical equation for the synthesis of Bi_2MoO_6 is shown below:

$$2Bi(NO_3)_3.5H_2O + Na_2MoO_4.2H_2O \rightarrow Bi_2MoO_6 + 2NaNO_3 + 4NO_2 + O_2 + 12H_2O \quad (1)$$

2.3. Characterization of the materials

An X-ray Diffraction (XRD) device (D8 Advance, Bruker, Germany) with Cu- Kα wavelength ($\lambda = 1.54060$ Å) was used to analyze the crystal structures of the composite. In addition, the morphological characterization of the prepared materials was achieved by a field emission scanning electron microscope (FE-SEM) (JSM-IT800/Jeol, Japan), which revealed the integration of g-C_3N_4/ Bi_2MoO_6 onto the Clinoptilolite surface. Furthermore, using a Spectrum Two instrument from PerkinElmer, USA, Fourier-transform infrared (FT-IR) analysis was used to confirm the presence of g-C_3N_4, Bi_2MoO_6, and Clinoptilolite in the CNBC. Moreover, depending on the N_2 adsorption-desorption measurements were analyzed by the Brunauer-Emmett-Teller (BET) analysis (ASAP2060 instrument from Micromeritics, USA) to determine the surface areas and pore size. An energy-dispersive X-ray (EDX) spectrometer (JEC-3000FC/Jeol, Japan) was used to analyze the CNBC material's elemental composition and perform element mapping. Transmission electron microscopy (TEM) images were obtained by JEOL Model JEM-F200 microscope.

2.4. Photocatalytic activity procedures transition batch to continuous system

The photocatalytic decomposition of OTC was performed at ambient temperature using a 40W L4X LED lamp emitting radiation at a wavelength of 446 nm. The batch system followed the configuration depicted in Figure 1a, while the continuous system adhered to the setup shown in Figure 1b. In the batch system, 50 mg of CNBC nanocomposite was mixed with 100 mL of 20 ppm OTC solution in a container that was lined with foil and was not see-through. The suspension was agitated in the dark for 30 minutes with continuous air bubbling in order to improve adsorption-desorption. The suspension was exposed to visible light for 90 minutes after adding 30 mg of $Na_2S_2O_8$. Each 15 minutes, 4 mL aliquots were centrifuged at 4000 rpm for 5

UNCORRECTED PROOF

minutes and filtered through a 0.22 µm PTFE syringe filter to remove photocatalyst particles. Each experiment was repeated three times.

A specific amount of photocatalyst was introduced into a tank containing 22 L of a 20 ppm OTC solution, followed by stirring to enhance adsorption. Subsequently, 30 mg of sodium persulfate was added to the initial tank. The mixture was then transferred into the photocatalytic system using a peristaltic pump, which allowed for precise adjustment of the flow rate. The continuous aeration was maintained throughout the process. The sampling began at 2 hours as this is the time required to fill the reactor (which has a volume of 8 liters and a flow rate of 4 liters per hour). At predetermined time intervals, 4 mL aliquots were collected, centrifuged for 5 minutes at 4000 rpm, and filtered through a 0.22 µm PTFE membrane to remove residual photocatalyst particles.

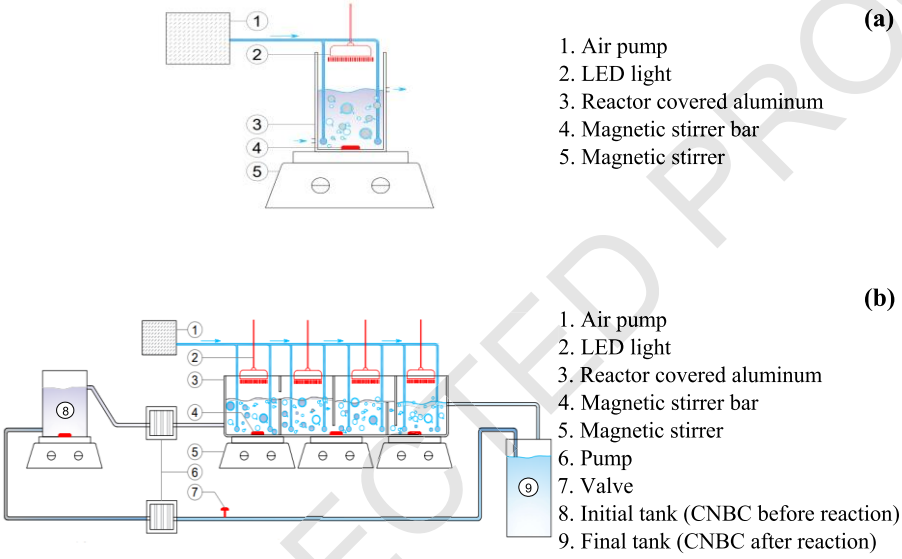

Figure 1. Photocatalyst degradation of OTC used for batch (a) and continuous (b) experiments setups

The concentration of OTC was measured using a UV-Vis spectrophotometer (Model SP-60, Biochrom, UK) at a wavelength of 355 nm, with a calibration curve ranging from 0-40 mg/L. The OTC degradation efficiency was calculated by Eq. (2):

$$H(\%) = (1 - \frac{C_t}{C_0})\, x\, 100 = (1 - \frac{A_t}{A_0})\, x\, 100 \quad (2)$$

where C_t and A_t are the concentration and absorbance of OTC at time t. C_0 and A_0 are the initial concentration and absorbance of OTC.

3. RESULT

3.1. Synthesis of material and its characterization

In the revised synthesis process, the tertiary nanocomposite material was produced at a large scale, with each batch yielding approximately 7.05 g ± 0.02 g, representing a synthesis efficiency of 97.86 %, based on the theoretical mass of 7.20 g. Figure 2a presents the crystal structure of the ternary nanocomposites (CNBC) as determined by XRD spectroscopy. It can be seen that Bi_2MoO_6 exhibited prominent diffraction peaks between at 2θ angles ranging from

UNCORRECTED PROOF

10.9° to 58.4°, which correspond to the (020), (131), (060), (151), (202), (133), and (191) crystal planes of Bi_2MoO_6 (JCPDS No. 21-0102). However, the characteristic peaks of g-C_3N_4 (13.1° and 27.5°) were not clearly observed in the composites due to the overlap between the (002) plane of g-C_3N_4 and the (131) plane of Bi_2MoO_6. Clinopilolite's characteristic peaks ((400), (002), (42-2), and (151)) were difficult to discern due to the presence of g-C_3N_4 and Bi_2MoO_6 on its surface. Notably, the XRD spectra of CNBC after the reaction were nearly identical to those of CNBC before the reaction, indicating that the crystal structure remained stable throughout the oxytetracycline OTC degradation process.

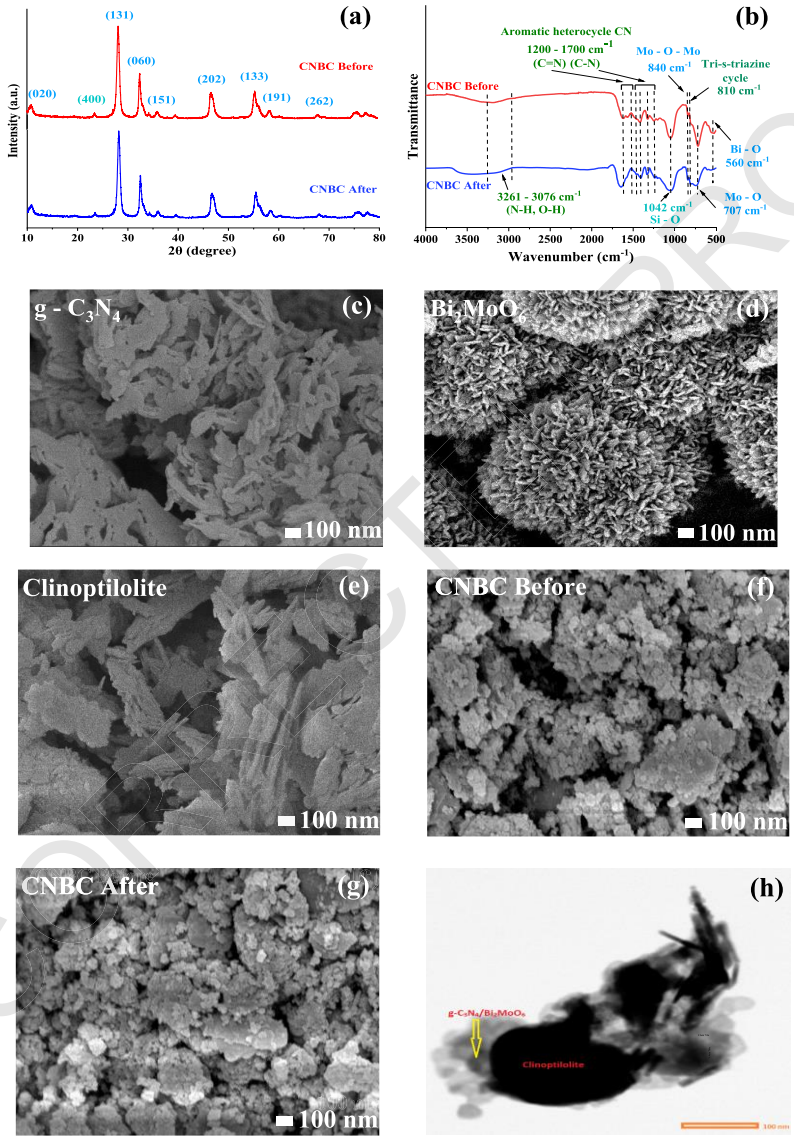

Figure 2. (a) XRD spectra, (b) FT-IR spectra, FE-SEM images of g-C_3N_4 (c), Bi_2MoO_6(d), Clinoptilolite (e), CNBC before the reaction (f) and CNBC after the reaction (g), and TEM image of CNBC before the reaction (h) with g-C_3N_4 (Green), Bi_2MoO_6 (Blue), and Clinoptilolite (Teal).

The chemical bonds within the CNBC material before the reaction and after the reaction were confirmed by FT-IR analysis (Figure 2b). In the g-C_3N_4 structure, the stretching vibrations

UNCORRECTED PROOF

of the N-H and O-H groups, associated with internal H_2O molecules, produced spectroscopic bands between 3076 cm^{-1} and 3261 cm^{-1} [20]. Additionally, aromatic stretching vibrations of C-N and C=N were observed between 1200 cm^{-1} and 1700 cm^{-1} [21], while the strong peak at 810 cm^{-1} corresponds to the ring breathing vibration of the tri-s-triazine cycles [21]. In Bi_2MoO_6, peaks at 560 cm^{-1}, 707 cm^{-1}, and 840 cm^{-1} were assigned to Bi-O, Mo-O, and Mo-O-Mo linkage within Bi_2MoO_6, respectively. Meanwhile, the peak at 1042 cm^{-1} was attributed to Si-O stretching in Clinoptilolite [22]. The FT-IR spectra of CNBC after the reaction were identical to those of CNBC after reaction, indicating that the photocatalyst's chemical composition and structure remain unchanged during OTC degradation. However, CNBC after the reaction exhibited increased peak intensity between 3076 cm^{-1} and 3261 cm^{-1}, suggesting a higher concentration of internal H_2O molecules.

Scanning electron microscopy (SEM) images of both single and composite materials are presented in Figures 2(c-g). Figure 2c reveals that g-C_3N_4 features a wrinkled, uneven layered structure, whereas Bi_2MoO_6 forms spherical, 3D flower-like crystals with diameters ranging from 1.0 to 1.3 μm, and the crystal edges are visible [23]. At higher magnifications, the microspheres of Bi_2MoO_6 appear to have spike-like protrusions, resembling the quills of a porcupine [24]. Additionally, the surface morphology of clinoptiolite includes multiple layers of smooth scales in a lamellar arrangement. Moreover, as shown in Figures 2(f-g), the morphology of both materials remains virtually unchanged before and after treatment.

Transmission electron microscopy (TEM) images of the CNBC nanocomposite before the reaction are displayed at a resolution of 100 in Figure 2h. The TEM images indicate a tight integration among g-C_3N_4/Bi_2MoO_6 and clinoptilolite within the heterogeneous three-component structure of CNBC. Such a favorable architecture suggests the high efficiency of the photocatalyst in the process of electron and hole separation generated by light exposure.

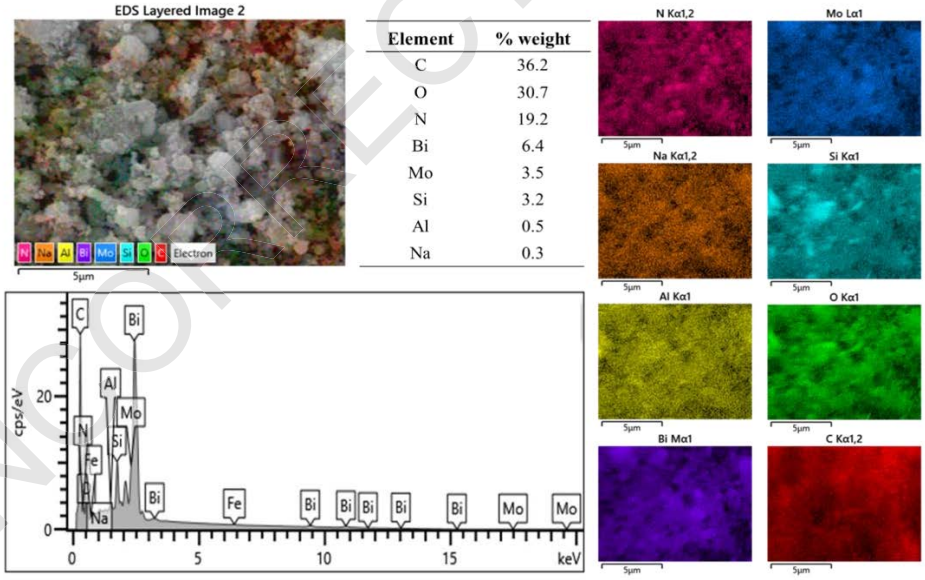

Figure 3. EDX spectra and its element mapping of CNBC material before the reaction.

In Figure 3, the elemental composition and mapping of the CNBC material before the reaction was analyzed using EDX spectroscopy. The presence and distribution of Si, Al, and Na confirm the existence of Clinoptilolite [25]. The g-C_3N_4 component was identified by the

UNCORRECTED PROOF

presence of C and N, while Bi_2MoO_6 was characterized by Bi, Mo, and O. The EDX spectra in Figure 3 revealed that these elements are uniformly distributed and dispersed, confirming that g-C_3N_4 and Bi_2MoO_6 are well coated on the surface of Clinoptilolite.

Further analysis through Brunauer-Emmett-Teller (BET) measurements revealed that the specific surface areas of g-C_3N_4 and Bi_2MoO_6 were 34.41 m^2/g and 37.14 m^2/g, respectively, while the HCl-activated Clinoptilolite showed a larger surface area of 75.76 m^2/g. Consequently, the specific surface area of the tertiary nanocomposite increased up to 59.57 m^2/g (Figure 4), which is higher than the 48.55 m^2/g reported in the earlier study [19]. The combination of g-C_3N_4/ Bi_2MoO_6 with Clinoptilolite enhanced the material's surface area, promoting effective adsorption and facilitating photocatalytic degradation on the material's surface.

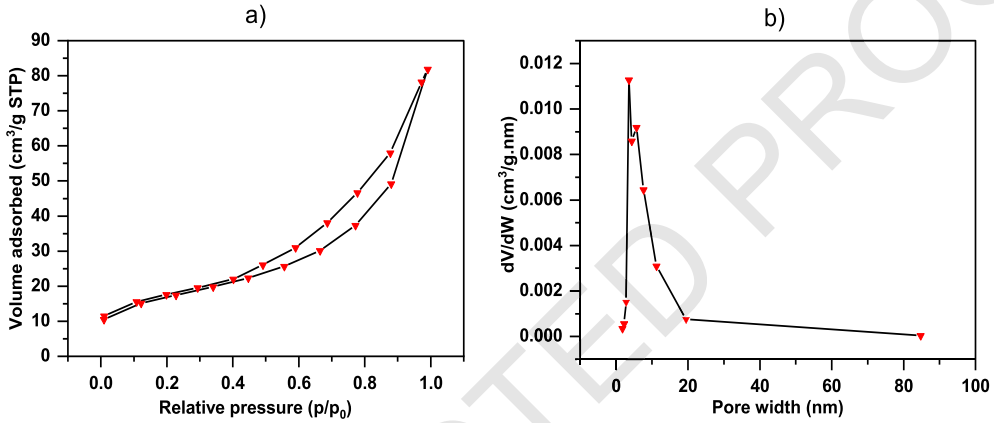

Figure 4. a) N_2 adsorption/desorption isotherms and b) Pore size distribution of CNBC before the reaction.

The optical properties of the materials were thoroughly investigated in a previous publication [19] using UV-Vis diffuse reflectance spectroscopy (DRS) and photoluminescence (PL) spectroscopy. The UV-Vis DRS analysis revealed that the band gaps of g-C_3N_4, Bi_2 MoO_6, g-C_3N_4/Bi_2MoO_6, and g-C_3N_4/Bi_2MoO_6/Clinoptilolite are 2.72, 2.07, 2.30, and 2.23 eV, respectively. These values indicate a narrowing of the band gap when clinoptilolite is added to the g-C_3N_4/Bi_2MoO_6 catalyst. Consequently, the C_3N_4/Bi_2MoO_6/Clinoptilolite demonstrates improved electron-hole pair separation capabilities, making it more beneficial for photocatalytic OTC activity compared to the binary catalyst. Furthermore, the PL results also indicate a decrease in photoluminescence intensity in the order of g-C_3N_4 > Bi_2MoO_6 > C_3N_4/Bi_2MoO_6/Clinoptilolite, leading to reduced recombination rates of electron-hole pairs within the three-component nanocomposite.

3.2. Effect of photocatalytic in batch system

The pH of a solution plays a pivotal role in pollutant degradation, as it directly influences the chemical configuration of the pollutants. This impact was illustrated by the photocatalytic degradation of OTC under visible light at varying pH levels (pH = 4, pH = 7, and pH = 11), as depicted in Figure 5a. The degradation efficiency exhibited only slightly variations, with 85.81 % efficiency at pH = 4, compared to 73.80 % at pH = 7, and 75.87 % at pH = 11. The pH of a

UNCORRECTED PROOF

solution affects the surface charge of the material, the existing forms of OTC (oxytetracycline), and the type of active oxygen species involved. At a pH of 4, the surface carries a positive charge, enhancing the adsorption of $S_2O_8^{2-}$ ions, which in turn boosts the activation of $S_2O_8^{2-}$ leading to increased degradation efficiency of OTC. At a pH of 11, there is a conversion of the $SO_4^{\bullet-}$ radicals into $^{\bullet}OH$ radicals, reducing the oxidation potential and consequently lowering the degradation efficiency of OTC. Ultimately, the highest degradation efficiency was observed at the initial pH of 4, with a value of 85.81 %, highlighting the optimal acidic conditions.

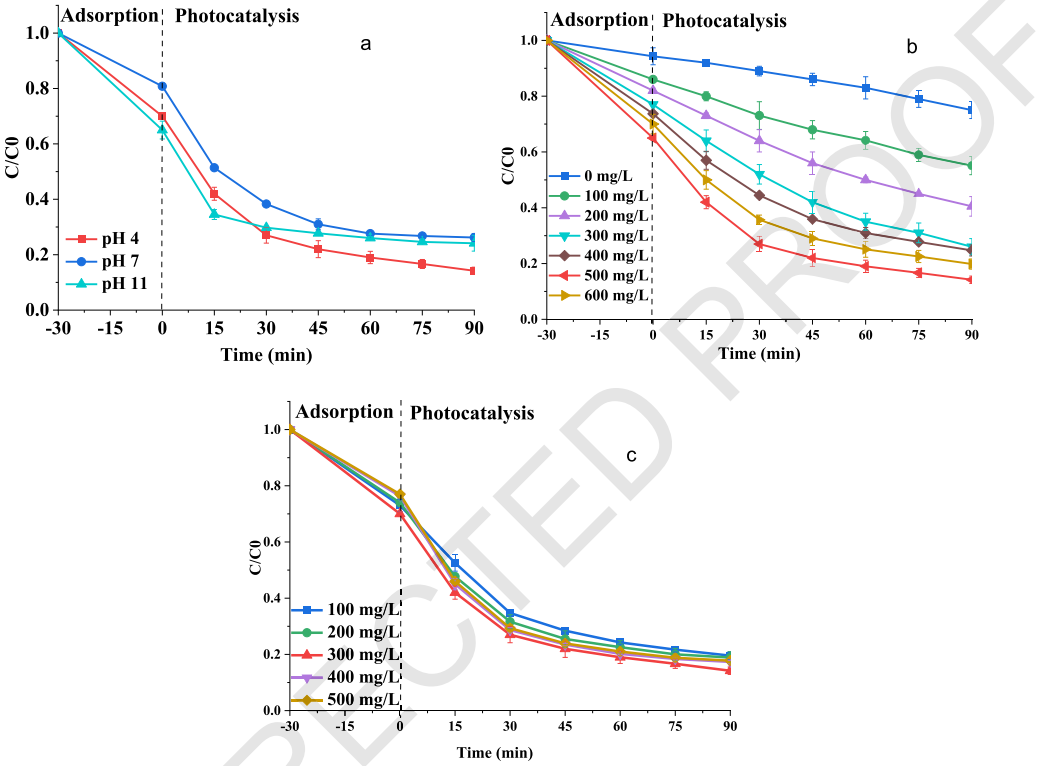

Figure 5. Efficiency curves of OTC with different pH (a); CNBC dosages (b); and $Na_2S_2O_8$ (c) under visible light irradiation in batch experiments.

Moreover, Figure 5b demonstrates that the content of CNBC has a significant impact on OTC degradation efficiency. In the absence of a catalyst, the degradation efficiency dropped to only 24.96 %, while it increased progressively 44.93 %, 59.50 %, 74.10 %, 75.30 %, and 85.81 % as the catalyst content ranged from 100 mg/L to 500 mg/L, it can be explained by the increase in the number of active sites on the catalyst. However, at 600 mg/L, the efficiency slightly decreased to 80.18 %. This decrease can be attributed to the catalyst shielding the light beam, thus limiting the reaction to the surface of the tertiary material. This finding underscores the critical role CNBC plays in the photocatalysis process.

Regarding the effect of sodium persulfate concentration, Figure 5c shows that its influence on OTC degradation is less pronounced compared to the catalyst dosage. Degradation efficiency increased from 78.57 % to 83.35 % as the $Na_2S_2O_8$ content rose from 100 mg/L to 300 mg/L, yielding efficiencies of 80.43 %, 81.13 %, and 85.81 %, respectively. This can be explained by the fact that higher concentrations of PDS generate more reactive oxygen species (ROS), while also inhibiting the recombination of electron-hole pairs, thereby enhancing the degradation

UNCORRECTED PROOF

efficiency of OTC. However, when the sodium persulfate content was further increased to 400 mg/L and 500 mg/L, the efficiency slightly decreased to 82.67 % and 82.25 %. The reduction can be attributed to the excess $SO_4^{\bullet-}$ radical transforming into $S_2O_8^{2-}$ or $S_2O_8^{-}$, which possess weaker oxidation properties than $SO_4^{\bullet-}$, as illustrated in Eqs. (3) and (4). Thus, 300 mg/L of $Na_2S_2O_8$ is identified as the optimal condition.

$$S_2O_8^{2-} + SO_4^{\bullet-} \rightarrow SO_4^{2-} + S_2O_8^{-} \quad (3)$$

$$SO_4^{\bullet-} + SO_4^{\bullet-} \rightarrow S_2O_8^{2-} \quad (4)$$

3.3. Effect of photocatalytic in continuous system

After identifying the best system settings for treating 20 ppm OTC with 500 mg/L catalyst, 300 mg/L $Na_2S_2O_8$, and unadjusted pH (pH = 4), the degradation efficiency reached 85.81 %. However, when the same conditions were applied to treat 20 ppm OTC with the continuous system, the efficiency decreased to 69.76 %, which was lower than the 82.24 % efficiency achieved by the sample without a catalyst. This reduction can be explained by the excessive quantity of catalyst, which inhibits light from accessing through the solution to the bottom of the reactor, causing the reaction to occur simply in the solution at the top. By reducing the catalyst amount to 250 mg/L and 150 mg/L, the efficiency gradually increased to 86.52 % and 93.46 %, respectively. As shown in Figure 6a, at a content of 150 mg/L, the efficiency reached its highest level at 93.46 %. This optimization reduces the catalyst requirement by more than threefold compared to the batch system and enables the treatment of larger volumes of water.

Simultaneously, the flow rate is critical in the continuous photocatalytic system as it determines the actual reaction time of the sample. As shown in Figure 6b, at a flow rate of 6 L/hour, the degradation efficiency after cycles 2 and 3 reached only 72.68 % - 84.10 %, whereas at flow rates of 3 L/hour and 4 L/hour, the efficiency increased to 89.12 % - 94.56 %. This indicates that a flow rate of 6 L/h is entirely unsuitable for the treatment of OTC in a continuous system. In contrast, the treatment efficiencies at 4 L/h and 3 L/h are comparable, demonstrating the potential for industrial-scale applications with the ability to treat large sample volumes in a single day. With the continuous photocatalytic system installed as depicted in the Figure 1b, the 3-component catalyst system can be effectively used for pilot-scale OTC treatment at a flow rate of 4 L/h.

The treatment capacity of the continuous system is evaluated based on the rate and effectiveness of OTC removal at varying concentrations. In this system, it took 1 hour to fill the tank, and the optimal conditions are 150 mg/L catalyst, 300 mg/L sodium persulfate, and unadjusted pH (pH = 4). As shown in Figure 6c, at a concentration of 5 ppm, the system reached 100 % efficiency after just 1 hour of initial treatment, with the OTC solution continuously processed while flowing through the system. At a concentration of 10 ppm, the time required for the system to reach 100 % efficiency extends considerably to 5 hours. Moreover, as the concentration was raised to 20 ppm, the processing time further escalates, reaching 9 hours to achieve 100 % efficiency. The UV-Vis spectra in Figure 6d support these findings, indicating that after 2 hours, the characteristic peak of OTC began to decline gradually, while absorbance in the 200–250 nm range rose significantly. After 10 hours, the peak corresponding to OTC at a wavelength of 354 nm disappeared entirely, signifying complete degradation of OTC. This indicates that OTC was decomposed into new intermediate compounds that were further broken down during the photocatalytic process with the CNBC material.

UNCORRECTED PROOF

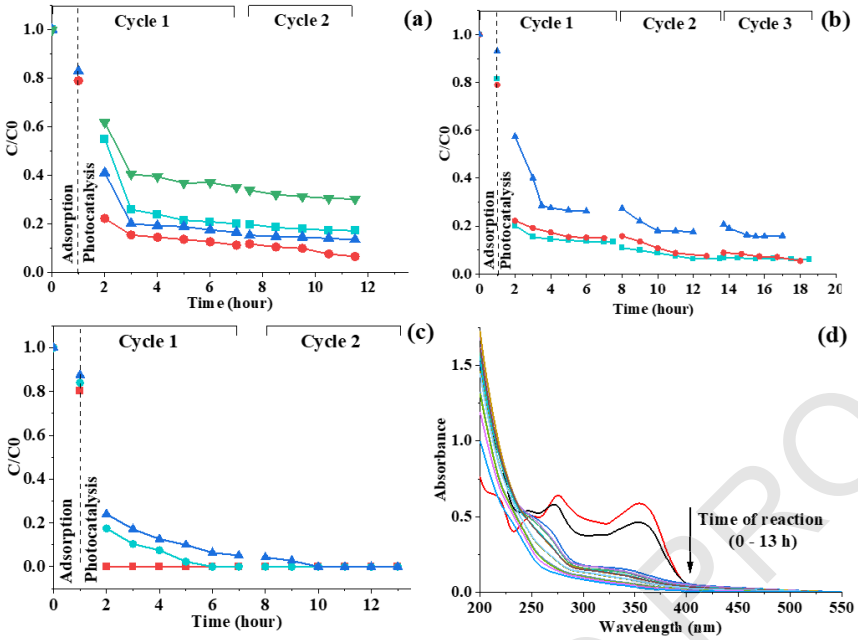

Figure 6. Efficiency curves of OTC at varying dosages of CNBC (a): 0 mg/L (■), 150 mg/L (●), 250 mg/L (▲), 500 mg/L (▼); different flow rates (b): 3 L/hour (■), 4 L/hour (●), 6 L/hour (▲); and different concentrations of OTC (c): 5 ppm (■), 10 ppm (●), 20 ppm (▲); along with the spectra of OTC at 20 ppm (d), under visible light irradiation during continuous system.

The degradation process of OTC (oxytetracycline) in the photocatalytic system occurs through various pathways involving the removal of hydroxyl, methyl, carbonyl, and amide groups, along with ring-opening reactions. This results in the formation of 25 degradation products, intermediate products with lower molecular weights, and ultimately mineralization to form stable inorganic products. These processes have been studied in detail in our previous research [19], where we explored the specific mechanisms and chemical transformations within the photocatalytic degradation of OTC. This comprehensive analysis helps to understand the efficiency and effectiveness of the photocatalyst in breaking down complex organic compounds into simpler, environmentally benign substances.

4. CONCLUSION

In this study, the updated g-C_3N_4/Bi_2MoO_6/Clinoptilolite nanocomposite was synthesized using a modified solvo-thermal process with increased precursor levels and solvent volume. The material demonstrated high photocatalytic activity and purity. Characterization by FT-IR, XRD, and FE-SEM confirmed the integration of g-C_3N_4/ Bi_2MoO_6 onto the surface of clinoptilolite, and indicated that the material remained stable after continuous photocatalytic degradation of OTC, while BET analysis showed a significant increase in surface area (59.57 m^2/g). Under optimized conditions in the batch system (500 mg/L CNBC, 300 mg/L $Na_2S_2O_8$, pH 4), 85.81 % OTC removal was achieved within 2 hours. In the continuous system, complete degradation with 100 % OTC removal was achieved using only 150 mg/L catalyst at a flow rate of 4 L/h. The continuous process demonstrated significant potential for industrial-scale applications in treating antibiotic-contaminated wastewater.

UNCORRECTED PROOF

Acknowledgement. The authors express their sincere gratitude for the financial support provided by the University of Science and Technology of Hanoi, Vietnam Academy of Science and Technology, under grant No. VAST07.03/23-24. Additionally, the authors extend their thanks to the Research Group "Sustainable Energy and Environmental Development (SEED)" for their invaluable support.

CRediT authorship contribution statement. Phuong Thu Le: Conceptualization, Methodology, Funding acquisition, Project administration, Resources, Supervision, Data curation, Visualization, Validation, Writing - Original Draft, Writing - Review & Editing; Ngoc Thanh Truc Nguyen: Investigation, Data curation, Formal analysis, Writing - Original Draft; Hong Nam Nguyen: Data curation, Formal analysis, Visualization, Validation; Trung Dung Nguyen: Methodology, Visualization, Validation; Thu Phuong Nguyen: Investigation, Data curation, Formal analysis; Tien Le: Data curation, Formal analysis; Thi Mai Thanh Dinh: Funding acquisition, Project administration, Resources, Writing - Review & Editing.

Declaration of competing interest. The authors declare that they have no known competing financial interests or personal relationships that could have appeared to influence the work reported in this paper.

REFERENCE

1. Papich M. G. – Oxytetracycline. In: *Papich Handbook of Veterinary Drugs* (Fifth Edition). St. Louis (MO), W.B. Saunders, (2021) 689–691.
2. Mog M., Ngasotter S., Tesia S., Waikhom D., Panda P., Sharma S., Varshney S. – Problems of antibiotic resistance associated with oxytetracycline use in aquaculture: A review. J. Entomol. Zool. Stud., **8** (2020) 1075–1082.
3. Pham D. K., Chu J., Do N. T., Brose F., Degand G., Delahaut P., De Pauw E., Douny C., Van Nguyen K., Vu T. D., et al. – Monitoring antibiotic use and residue in freshwater aquaculture for domestic use in Vietnam. EcoHealth, **12** (2015) 480–489. https://doi.org/10.1007/s10393-014-1006-z.
4. Ström G. H., Björklund H., Barnes A. C., Da C. T., Nhi N. H. Y., Lan T. T., Magnusson U., Haldén A. N., Boqvist S. – Antibiotic use by small-scale farmers for freshwater aquaculture in the upper Mekong Delta, Vietnam. J. Aquat. Anim. Health, **31** (2019) 290–298. https://doi.org/10.1002/aah.10084.
5. Jankowska A., Ejsmont A., Galarda A., Goscianska J. – The outcome of human exposure to environmental contaminants. Importance of water and air purification processes. In: Tyagi I., Goscianska J., Dehghani M. H., Karri R. R., eds. *Sustainable Materials for Sensing and Remediation of Noxious Pollutants*. Elsevier, (2022) 15–37. https://doi.org/10.1016/b978-0-323-99425-5.00003-7.
6. Do T. C. M. V., Nguyen D. Q., Nguyen T. D., Le P. H. – Development and validation of a LC-MS/MS method for determination of multi-class antibiotic residues in aquaculture and river waters, and photocatalytic degradation of antibiotics by TiO_2 nanomaterials. Catalysts, **10** (2020) 356. https://doi.org/10.3390/catal10030356.
7. Binh V. N., Dang N., Anh N. T. K., Ky L. X., Thai P. K. – Antibiotics in the aquatic environment of Vietnam: Sources, concentrations, risk and control strategy. Chemosphere, **197** (2018) 438–450. https://doi.org/10.1016/j.chemosphere.2018.01.061.
8. Huong L. Q., Hang T. T. T., Ngoc P. T., Tuat C. V., Erickson V. I., Padungtod P. – Pilot monitoring of antimicrobial residues in chicken and pork in Vietnam. J. Food Prot., **83** (2020) 1701–1706. https://doi.org/10.4315/jfp-20-111.
9. Wang Z., Du Y., Yang C., Liu X., Zhang J., Li E., Zhang Q., Wang X. – Occurrence and ecological hazard assessment of selected antibiotics in the surface waters in and around Lake Honghu, China. Sci. Total Environ., **609** (2017) 1423–1432. https://doi.org/10.1016/j.scitotenv.2017.08.009.
10. Li H., Liu J., Hou W., Du N., Zhang R., Tao X. – Synthesis and characterization of g-C_3N_4/Bi_2MoO_6 heterojunctions with enhanced visible light photocatalytic activity. Appl. Catal. B: Environ., **160–161** (2014) 89–97. https://doi.org/10.1016/j.apcatb.2014.05.019.
11. Tang J., Shi T., Wu X., Cao H., Li X., Hua R., Tang F., Yue Y. – The occurrence and distribution of antibiotics in Lake Chaohu, China: Seasonal variation, potential source and risk assessment. Chemosphere, **122** (2015) 154–161. https://doi.org/10.1016/j.chemosphere.2014.11.032.

UNCORRECTED PROOF

12. Li L., Liu D., Zhang Q., Song K., Zhou X., Tang Z., Zhou X. – Occurrence and ecological risk assessment of selected antibiotics in the freshwater lakes along the middle and lower reaches of Yangtze River basin. J. Environ. Manage., **249** (2019) 109396. https://doi.org/10.1016/j.jenvman.2019.109396.
13. Tran Q. M., Le P. T., Nguyen T. P., Nguyen H. N., Do T. H., Nguyen T. D., Dinh T. M. T. – Efficient removal of emerging pollutant oxytetracycline by cost-effective biochar–hydroxyapatite composite. Asia-Pac. J. Chem. Eng., **19** (2024) e3124. https://doi.org/10.1002/apj.3124.
14. Wang X., Wang H., Li F., Hu X., Xie Z., Hua T. – Activation of peroxymonosulfate in an electrochemical filter by $MnFe_2O_4$-rGO electro-assisted catalytic membrane for the degradation of oxytetracycline. J. Environ. Chem. Eng., **10** (2022) 107008. https://doi.org/10.1016/j.jece.2021.107008.
15. Cheng X., Guan R., Chen Y., Qian Y., Shang Q., Sun Y. – Adsorption and photocatalytic degradation process of oxytetracycline using mesoporous Fe-TiO_2 based on high-resolution mass spectrometry. Chem. Eng. J., **460** (2023) 141618. https://doi.org/10.1016/j.cej.2023.141618.
16. Alves D. C. da S., de Farias B. S., Breslin C., de Almeida Pinto L. A., Cadaval T. R. S. – Carbon nanotube-based materials for environmental remediation processes. In: Giannakoudakis D., Meili L., Anastopoulos I., eds. *Advanced Materials for Sustainable Environmental Remediation*. Elsevier, (2022) 475–513. https://doi.org/10.1016/b978-0-323-90485-8.00017-5.
17. Hu G., Ren X., Meng D., Gao D., Guo Q., Hu X., Wang L., Song J. – Facile fabrication of S-scheme Bi_2MoO_6/g-C_3N_4/sepiolite ternary photocatalyst for efficient tetracycline degradation under visible light. Mater. Sci. Semicond. Process., **166** (2023) 107712. https://doi.org/10.1016/j.mssp.2023.107712.
18. Jing L., Xu Y., Xie M., Wu C., Du X., Zhao H., Zhong N., Li H., Gates I. D., Hu J. – The enhanced visible-light-driven porous O/P-C_3N_4 for persulfate photoactivation: Enhanced removal of refractory pollutants and lignin valorization. Chem. Eng. J., **482** (2024) 149090. https://doi.org/10.1016/j.cej.2024.149090.
19. Le P. T., Nguyen T. P., Do T. H., Nguyen H. N., Dinh T. M. T., Phan T. T., Tsubota T., Nguyen T. D. – Synergistic effect of the heterojunction g-C_3N_4/Bi_2MoO_6/clinoptilolite to enhance the photocatalytic degradation of antibiotics in water in the presence of persulfate. Environ. Sci.: Water Res. Technol., **10** (2024) 2665–2687. https://doi.org/10.1039/d4ew00549j.
20. Narkbuakaew T., Sujaridworakun P. – Synthesis of tri-S-triazine based g-C_3N_4 photocatalyst for cationic rhodamine B degradation under visible light. Top. Catal., **63** (2020) 1086–1096. https://doi.org/10.1007/s11244-020-01375-z.
21. Xu H., Zhang T., Wang D., Cai D., Chen S., Wang H., Shu S., Zhu Y. – Degradation of tetracycline using persulfate activated by a honeycomb structured S-doped g-C_3N_4/biochar under visible light. Sep. Purif. Technol., **300** (2022) 121833. https://doi.org/10.1016/j.seppur.2022.121833.
22. Zhou P., Shen Y., Zhao S., Chen Y., Gao S., Liu W., Wei D. – Hydrothermal synthesis of novel ternary hierarchical MoS_2/TiO_2/clinoptilolite nanocomposites with remarkably enhanced visible light response towards xanthates. Appl. Surf. Sci., **542** (2021) 148578. https://doi.org/10.1016/j.apsusc.2020.148578.
23. Liu N., Dang Y., Hu B., Tian M., Jiang H., Quan G., Qiao R., Lei J., Zhang X. – BN/Fe_3O_4/MIL-53(Fe) ternary nanocomposite for boosted ibuprofen degradation by visible light assisted photocatalytic activation of persulfate. Surf. Interfaces, **35** (2022) 102472. https://doi.org/10.1016/j.surfin.2022.102472.
24. Li N., Gao H., Wang X., Zhao S., Lv D., Yang G., Gao X., Fan H., Gao Y., Ge L. – Novel indirect Z-scheme g-C_3N_4/Bi_2MoO_6/Bi hollow microsphere heterojunctions with SPR-promoted visible absorption and highly enhanced photocatalytic performance. Chin. J. Catal., **41** (2020) 426–434. https://doi.org/10.1016/s1872-2067(19)63478-9.
25. Biblioteca I., Sambucci M., Valente M. – Zeolite-clinoptilolite conditioning for improved heavy metals ions removal: A preliminary assessment. Ceram. Int., **49** (2023) 39649–39656. https://doi.org/10.1016/j.ceramint.2023.09.319.

UNCORRECTED PROOF